Nanopore-filling effect of phenanthrene sorption on modified black carbon

Shujie Hu [a,b], Dainan Zhang [a], Yongqiang Xiong [a], Yu Yang [a], Yong Ran [a,*]
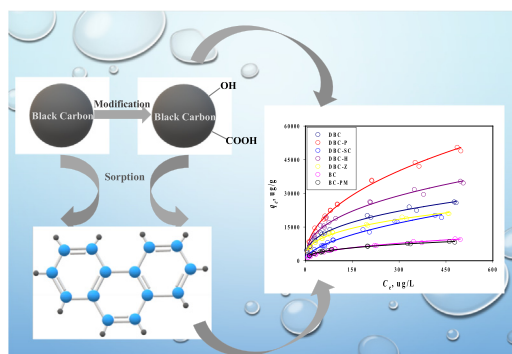
[a] State Key Laboratory of Organic Geochemistry, Guangzhou Institute of Geochemistry, Chinese Academy of Sciences, Guangzhou 510640, China
[b] University of Chinese Academy of Sciences, Beijing 100049, China

HIGHLIGHTS

- Modification changed the nanoporosity and sorption behavior of black carbon.
- The sorption affinity is higher for H_2O_2 oxidation than for other treatments.
- Sorption affinity of phenanthrene is positively related to nanoporosity.
- Nanopore-filling was the main mechanism for the sorption of phenanthrene.
- The molecular sieve effect can affect the nanopore filling volumes.

GRAPHICAL ABSTRACT

ABSTRACT

Black carbon was produced by slow pyrolysis under an oxygen-limited condition at 500 °C, and was modified by some chemical methods (oxidation, hydrolysis, activation, and surface recombination). The modified samples were characterized by using elemental analysis, Fourier transformed infrared spectroscopy (FTIR), X-ray photoelectron spectroscopy (XPS) surface analysis, Boehm titration, cation exchange capacity(CEC)analysis, CO_2 adsorption analysis, and then used to investigate the sorption behavior of phenanthrene. The results showed that the activation of $ZnCl_2$ gave a maximum nanopore volume of 96.5 μL/g and a specific surface area of 241 m^2/g, while the oxidation of NaClO gave a minimum nanopore volume of 63.3 μL/g and a specific surface area of 158 m^2/g. The FTIR, XPS, and Boehm titration analysis showed that the new oxygen-containing functional groups were introduced during the oxidation treatments of H_2O_2 and NaClO. The sorption of phenanthrene on all samples was typically nonlinear, and the nonlinear factor (n) was negatively correlated with V_o, especially with V_o at 0–1.1 nm. The sorption parameter (log K_{OC}) was positively correlated with nanopore volume (V_o) and specific surface area (SSA). Moreover, the model analysis showed that the nanopore filling was the main sorption mechanism, and molecular sieve effect was observed in the sorption of phenanthrene.

© 2018 Elsevier B.V. All rights reserved.

1. Introduction

Black carbon (BC) is a carbonaceous residue produced by the incomplete combustion of biomass or fossil fuels (Guo et al., 2016; Schmidt and Noack, 2000; Zhang et al., 2011; Zhu et al., 2005), with high carbon content and relatively small amount of polar functional groups. The

sorption of BC to hydrophobic organic contaminants (HOCs) is nonlinear, and the sorption capacity is much higher than that of natural organic matter (Accardi-Dey and Gschwend, 2002; Xu et al., 2010). Topically, the strong sorption capacity of black carbon could be caused by the following reasons. Firstly, the interaction between HOCs and black carbon is affected by the hydrophobic interaction (Chun et al., 2004; Zhu and Pignatello, 2005). Secondly, there are three kinds of sorption sites in black carbon: surface adsorption sites with planar structure and higher contents of aromatic functional groups, nanoscale micropores, and occlusion sites inside black carbon (Gustafsson et al., 1996; Jonker and Koelmans, 2002; Nguyen et al., 2007). Particularly, the nanopore-filling mechanism has been studied intensively in recent years. Previous investigations illustrated that the nanopore-filling mechanism is prominent for the sorption of HOCs (Ran et al., 2013; Sun et al., 2013). Nanopore-filling of HOCs can account for 45–98% of total sorption by peat and soil and 36–65% by kerogen (Ran et al., 2004; Zhang et al., 2014).

Recently, BC has received extensive attention due to the potential impact on improving soil fertility and sequestering carbon, as well as a potential low-cost adsorbent to control the migration of contaminants (Cheng et al., 2014; Guo et al., 2016). In addition, some researchers have chemically modified black carbon to change its chemical properties and structural characteristics, and to investigate its sorption mechanism. Through modification of the surface and regulation of the nanopore structure, the application of biocarbon materials in catalysis, energy storage, and environmental protection is more extensive (Liu et al., 2015). For example, previous study had carried out hydrolysis and oxidation modification on BCs, as a result of introducing new functional groups and changing the pore size distribution of BCs (Zhang et al., 2011). He et al. (2013) produced activated carbon at 850 °C with surface area up to 1442 m^2/g by using zinc chloride from rice straw. High storage capacity materials can store low-cost, clean renewable solar, wind, and biomass energy, which can attenuate the issues of environmental pollution and global warming (Linares et al., 2014).

Acid hydrolysis, oxidation, activation treatments, and surface recombination are common modification methods that have been successively used to modify black carbon and to explore mechanism of HOCs sorption (Mohanty et al., 2005; Zhang et al., 2011). First of the all, the acid hydrolysis can remove young biodegradable compounds such as proteins and polysaccharides, while more intractable macromolecules such as long chain alkyls and aromatic compounds are left behind (Paul et al., 2008). HCl (Paul et al., 2008; Zhang et al., 2011) and H$_3$PO$_4$ (Ahmedna et al., 2004; Girgis et al., 2002) are commonly used for this purpose. Secondly, the oxidation treatment can introduce oxygen-containing functional groups such as C═O, OH and COOH, which are important to improve the properties of black carbon. For example, OH and COOH can be associated with heavy metals by hydrogen bonding and complexation, which can significantly improve the adsorption capacity of heavy metals on BC (Liu et al., 2015). In addition, the surface oxygen-containing functional groups can improve the hydrophilicity of BC (Liu et al., 2015), which facilitates its dispersion in the aqueous phase and the adsorption of contaminants in the aqueous phase. NaClO and H$_2$O$_2$ are normally used as oxidants in previous reports (Lutfalla et al., 2014; Mikutta and Kaiser, 2011; Siregar et al., 2005). Thirdly, activation is primarily used to control the porosity of BC and to improve its surface area. ZnCl$_2$ as a mild Lewis acid, is a commonly used chemical activator (Ahmadpour and Do, 1997; Di Blasi et al., 2015). The mechanism of ZnCl$_2$ activation is its dehydration during pyrolysis (Liu et al., 2015). Dehydration process can obviously reduce the pyrolysis temperature of cellulose, hemicellulose, lignin, and other biomass components, and change their pyrolysis pathway by inhibiting the formation of bio-oil, and these processes promote the formation of pores. Finally, surface recombination can affect black carbon-based nanocomposites with mixed properties, opening up their potential applications in many fields. Surface recombination includes the in situ loading of metal nanoparticles and the post-incorporation of inorganic

nanostructures (Liu et al., 2015). Manganese oxide is a commonly used surface recombination agent (Song et al., 2014). However, the effects of structure and composition of black carbon on the nanopore volume and nanopore size distribution, as well as the effects of different modification methods, are ambiguous. In addition, the underestimation of the nanopore filling volumes by the molecular sieve effect needs further investigation (Duan et al., 2018). The relationship between the structure, composition, surface polarity of black carbon and its sorption mechanism with HOCs also needs further study (Chefetz and Xing, 2009; Ran et al., 2013; Wang et al., 2014; Zhu et al., 2005).

In this study, the Maoming oil shale is the bulk sample, which is an ancient biological organic matter. The sample was used to produce black carbon at 500 °C. Black carbon was modified by NaClO and H$_2$O$_2$ oxidation, ZnCl$_2$ activation, HCl hydrolysis, and KMnO$_4$ surface recombination, respectively. Chemical modification is mainly focusing on a series of sorbents with excellent sorption capacity and with a given amounts of functional —OH, and —COOH groups. Then, the structure and nanopore properties of the samples are related to the sorption mechanism of Phen. We recently found that the microporosity and specific surface areas of BC could be highly underestimated by the traditional N$_2$ adsorption technique (Zhang et al., 2014; Duan et al., 2018). Its sorption mechanism needs more investigations. The objectives of this study were: 1) to study the change of nanopores and organic functional groups before and after the modification, and 2) to study the sorption behavior of phenanthrene before and after the modification, as well as 3) to investigate the mechanism of the phenanthrene sorption by the BC and its modified samples.

2. Material and methods

2.1. Sample collection and treatments

Oil shale was collected from the Maoming city, Guangdong Province. The air-dried sample was ground to pass through a 60-mesh sieve and stored in an argon-filled glass container. The black carbon was produced by slow pyrolysis under an oxygen-limited condition as previously reported (Zhang et al., 2014). Briefly, 5 g of the powered sample was sealed in a steel ampoule. Before pyrolysis, the headspace was purged with N$_2$ for at least 1 min prior to sealing the steel ampoule. Four ampoules were heated in a temperature programing muffle furnace (20 °C/min from 25 °C to 200 °C and followed by 2 °C/min to 500 °C). After thermal treatment, the products were mixed and ground, and this sample was named as BC. The bulk sample was named as MB. Minerals of MB and BC were dissolved by with 1 M HCl/10% HF (Ran et al., 2007; Zhang et al., 2014). Specifically, carbonates were first dissolved in 1 M HCl for 24 h. The residual fraction was treated with 1 M HCl/10% HF for 5 d, which was repeated two times. After removing the second supernatant, the residue was washed with distilled water until neutral condition, then freeze-dried, and ground again. The demineralized samples were named as DMB and DBC, respectively.

DBC was treated with oxidization agents (H$_2$O$_2$, NaClO), acid agent (HCl), and activation agent (ZnCl$_2$), respectively, and BC was treated with surface recombination agent (KMnO$_4$). The NaClO treatment was modified based on previous studies (Paul et al., 2008; Siregar et al., 2005). In brief, two 0.3 g subsamples of DBC were each mixed with 30 mL of 6% NaClO and adjusted with concentrated HCl to pH 8. After 6 h of shaking at 25 °C and 125 rpm, the supernatant was discarded after centrifugation (1445g). The NaClO treatment was repeated three times. Then, the NaClO-treated samples were washed with 1 M NaCl and deionized water until chloride free (electrical conductivity <40 μS cm^{-1}), freeze-dried, weighted, and ground again, which was named as DBC-SC. Activation with ZnCl$_2$ was followed by the reported method (Shi et al., 2014). Two 0.3 g subsamples of the DBC were each mixed with 30 mL of 5 mol/L ZnCl$_2$ and shaken for 24 h at 25 °C and 125 rpm. The activation samples were washed with 3 M HCl and distilled water, then freeze-dried, weighted, and ground again, which

was named as DBC-Z. H_2O_2 treatment was based on the previous method (Zhang et al., 2011). Two 0.3 g subsamples of the DBC were each mixed with 30 mL of 10% H_2O_2 and shaken for 24 h (25 °C, 125 rpm). Acid hydrolysis was referred to the previous study (Zhang et al., 2011). Two 0.3 g subsamples of DBC were each mixed with 30 mL of 6 M HCl and shaken for 6 h (25 °C, 125 rpm). Surface recombination with $KMnO_4$ based on the previous research (Song et al., 2014). Two 2 g subsamples of BC were each mixed with 30 mL of $KMnO_4$ solution, and the weight ratio of $KMnO_4$ to BC was 1:10. The suspension was ultrasonically for 2 h and oven dried at 80 °C, and then the mixture was heated at 500 °C for 0.5 h. The H_2O_2-treated, HCl-treated, and $KMnO_4$-treated samples were washed with distilled water until neutral condition, freeze-dried, weighted, and ground again. These samples were named as DBC-P, DBC-H, and BC-PM, respectively.

2.2. Characterization of the black carbon and modified samples

C, H, N contents of the samples were measured by using a Vario EL CUBE elemental analyzer (Elementar, Germany), and O contents were analyzed with a Vario ELIII elemental analyzer (Elementar, Germany). The CO_2 isotherms were measured at 273 K using a Micromeritics ASAP 2460 surface area and pore size analyzer at 1×10^{-6} to 0.03 relatively atmospheric pressure. The surface areas (SSA) and nanopore volumes (V_o) were calculated using the *DR* (Dubinin-Radushkavich) model (Ran et al., 2013; Zhang et al., 2016), and the nanopore size distribution was estimated with density functional theory (DFT). In addition, in order to compare our investigation with previous investigations, we also used the nonlocal density functional theory (NLDFT) model to calculate the surface area. 0.1 mg of black carbon and its modified samples were milled with 80 mg of spectrally pure KBr pellets, respectively, and analyzed using Bruker VERTEX-70 Fourier Transform Infrared Spectrometer at a region of 400–4000 cm^{-1} and at resolution of 4 cm^{-1}. Moreover, the surface elemental composition (C, N, O, Si, and Al) and carbon-based functional groups of the black carbon and its modified samples were measured by X-ray photoelectron spectroscopy (XPS), a K-Alpha instrument (Thermo Fisher, Britain). Both the whole spectra (0–1200 ev) (resolution of 1 ev) and narrow ones of the above five elements (resolution of 0.05 ev) were recorded, and the XPS spectra were deconvoluted to separately identify the C-bonded O species and different C forms. The surface amphoteric property of the samples was evaluated by Boehm titration (Boehm, 1994; Chun et al., 2004; Zhang et al., 2011). The cation exchange capacities (CEC) of the samples were determined by a $BaCl_2$-H_2SO_4 method (ISO 11260–1997, 1997).

2.3. Batch sorption experiments

Phenanthrene (>98%), which is a typical hydrophobic organic pollutant, was purchased from Aldrich Chemical Co. Its log K_{OW} is 4.57 and the solubility in water is 1.12 mg/L. The concentrations of the original stock solutions were 100, 1000 and 5000 mg/L. The background solution (pH = 7) contained 0.01 mol/L $CaCl_2$, 200 mg/L NaN_3 and 5 mg/L $NaHCO_3$. All sorption isotherms were obtained using a given amount of sorbent (0.1–2.85 mg) and a batch equilibration technique in 50 mL glass ampules at 25 ± 1 °C, 125 rpm. Batch phenanthrene sorption by the black carbon and its modified samples were performed as described in previous reports (Zhang et al., 2016; Zhang et al., 2013; Zhang et al., 2015), and described in detail in Supplemental Data.

2.4. Sorption models

The Freundlich model (FM) was used to describe the sorption isotherms. K_{OC} is the sorption coefficient of organic compounds in soils or sediments and was used in the results and discussions. In addition, the Polanyi−Dubinin (*PD*) model, combined linear partitioning and Polanyi−Dubinin (*LPPD*) model, and Dubinin-Radushkevitch (*DR*) model (Kleineidam et al., 2002; Ran et al., 2004) were employed to describe

adsorption from aqueous solutions on nanopore solids. These models were listed in Supplemental Data.

3. Results

3.1. Compositions and elemental ratios of the samples

The weights and organic carbon (OC) recoveries of the modified BC and DBC were listed in Table S1. The yields after modification ranged from 78.8% to 119%, and the mass balance of OC ranged from 68.3% to 101%. In general, the oxidation treatment and surface recombination resulted in a large loss of OC (DBC-P was 31.7%, DBC-SC was 9.4%, and BC-PM was 8.5%), while the hydrolysis and activation treatment remained essentially constant. The elemental compositions of black carbon were presented in Table 1 and Table S2. MB had the highest ratio of H/C, while a significant decrease in ratio of H/C occurred in BC. In addition, the ratios of O/C decreased from 0.27 (MB) to 0.22 (BC). Compared with MB and BC, DMB and DBC had higher total organic carbon (TOC) contents, increasing from 50.5% to 68.1% and from 48.5% to 71.6%, respectively. For the modified DBC samples, the values of (N + O)/C were higher than those of DBC. For DBC-SC and DBC-P, (N + O)/C values increased from 0.18 to 0.38. In addition, the O/C values and O contents increased from 0.14 to 0.35 and from 13.6% to 28.5%, respectively. Moreover, the total organic carbon contents decreased from 71.6% to 54.5%. DBC-H showed a slight decrease of H/C and a mild increase of C/N. For DBC-Z, the C contents and H/C values showed slight decrease, while O contents and O/C values increased. After the surface recombination with $KMnO_4$, the contents of C and the H/C ratios decreased significantly from 48.5% to 43.3% and from 0.70 to 0.58, respectively. However, the contents of O and the O/C ratios decreased slightly.

3.2. Structure and surface properties of the samples

Fig. 1 showed the Infrared Spectrometer of black carbon and its modified samples. For the DBC-SC and DBC-P samples, a stronger absorption peak at 1714 cm^{-1} was observed in comparison with the DBC sample, which is the stretching vibration absorption peak for C=O. The C=O functional group of the DBC-SC sample was stronger than that of the DBC-P sample. Besides, these two samples simultaneously showed a stretching vibration absorption peak of C—O at 1400 cm^{-1}. Moreover, the C—O absorption peak at 1244 cm^{-1} and the hydroxyl-functional absorption peak at 3436 cm^{-1} were stronger for the DBC-SC or DBC-P samples than for the DBC sample. But the absorption peaks of methyl C—H at 2920 cm^{-1} and methylene C—H at 2846 cm^{-1} were significantly attenuated. However, the C=C stretching vibration of aromatic ring at 1600 cm^{-1} was insignificantly changed. For the DBC-H sample, the absorption peak of C=C stretching vibration of aromatic ring at 1600 cm^{-1} were significantly weakened, and no absorption peak appeared at 3436 cm^{-1}. The absorption peak of the hydroxyl functional group at 3436 cm^{-1} was enhanced in the DBC-Z sample, and no absorption peak appeared at 2920 cm^{-1} and 2846 cm^{-1}, and a broad peak appeared at 750 cm^{-1}, which is the C−H out-of-plane bending vibration absorption.

Compared with DBC, BC showed obvious absorption peaks at 472 cm^{-1}, 540 cm^{-1}, 1035 cm^{-1}, 3617 cm^{-1}, and 3693 cm^{-1}. 472 cm^{-1} was probably Si—O—Si bending vibration absorption peak, 1035 cm^{-1} may be the absorption peak of Si—O and polysaccharide C—O, and 3617 cm^{-1} may be the free vibration absorption peak of free hydroxyl. After the surface recombination by $KMnO_4$, the absorption peaks at 472 cm^{-1}, 540 cm^{-1}, 1035 cm^{-1}, 3617 cm^{-1} and 3693 cm^{-1} for BC-PM were all weakened, and absorption peak at 2920 cm^{-1} and 2846 cm^{-1} disappeared. However, there was a distinct absorption peak at 1102 cm^{-1} for BC-PM, which is probably due to C—O absorption peaks of esters or lactones.

Fig. S1 and Fig. S2 were the X-ray photoelectron spectra (XPS) with elemental survey scanning and C1s spectra scanning, respectively.

Table 1
Elemental compositions and chemical properties of the black carbon and its modified samples.

Sample	Elemental composition					Surface composition					Surface amphoteric properties (mmol/g)		CEC (cmol/kg)
	C%	O%	H/C	O/C	(N + O)/C	C%			[b]O/C	[c](N + O)/C	Acidic groups	Basic groups	
						C—C	C—O	COO					
MB	50.5	18.2	1.32	0.27	0.29	–	–	–	–	–	–	–	–
DMB	68.1	19.7	1.13	0.22	0.25	–	–	–	–	–	–	–	–
R500[a]	80.7	5.00	0.52	0.05	0.09								
DBC	71.6	13.6	0.63	0.14	0.18	81.6	6.08	2.02	0.04	0.07	8.69	nd	134
DBC-P	62.0	28.5	0.65	0.34	0.38	74.7	7.29	3.87	0.09	0.11	10.3	nd	188
DBC-SC	54.5	25.6	0.63	0.35	0.38	73.6	7.87	4.01	0.09	0.11	10.9	nd	149
DBC-H	71.8	15.0	0.53	0.16	0.19	88.1	4.53	0.00	0.04	0.05	8.35	nd	125
DBC-Z	68.1	15.6	0.55	0.17	0.21	87.4	4.33	0.00	0.04	0.05	8.47	nd	107
BC	48.5	14.3	0.70	0.22	0.25	67.6	3.17	0.00	0.12	0.14	1.85	8.42	99.5
BC-PM	43.3	12.2	0.58	0.21	0.24	76.9	3.62	0.00	0.07	0.08	1.43	6.96	120

[a] R500 was the BC samples in our previous investigation, which was exhaustively extracted with three-member solvents (Zhang et al., 2014; Duan et al., 2018).

[b] O/C ratios are the values corrected by the portion of oxygen that is originated from SiO_2.

[c] (N + O)/C ratios are the values corrected by the portion of oxygen that is originated from SiO_2.

Fig. S1 showed that carbon and oxygen were the major surface elements of black carbon and its modified samples. The deconvolution of the C1s produced three peaks: the peak at 284.8 eV was assigned to C—C, C=C, and C—H bonds, that at ~286.6 eV to C—O, and that at ~288.6 eV to COO. Table 1 and Table S2 listed the surface element compositions and surface functionalities of black carbon and its modified samples. Particularly, the contents of elements were the relative proportion of these five investigated elements, and the contents of C species were the relative proportion of the three deconvoluted C species.

For the DBC sample, the H_2O_2 and NaClO oxidation obviously strengthened the surface oxygen-containing functional groups, with C—O contents increasing from 6.08% to 7.87% and COO contents increasing from 2.02% to 4.01%, respectively. In addition, the surface oxygen contents increased from 6.01% to 11.2%. The HCl hydrolysis and the $ZnCl_2$ activation enhanced the surface C contents reaching 92.6% and reduced the C—O contents reaching 4.33%. Moreover, no COO appeared in DBC-H and DBC-Z. For the BC sample, the $KMnO_4$ surface recombination enhanced the surface C contents and C—O contents and reduced the surface O and Si contents. The surface polarity ((N + O)/C) of all the samples ranged from 0.05 to 0.21 and O/C ranged from 0.04 to 0.19, and was lower than that derived from elemental analysis (Table S2). However, when the inorganic oxygen from SiO_2 were deducted, the (N + O)/C values ranged from 0.05 to 0.14 and the O/C values ranged from 0.04 to 0.12 (Table 1).

The surface amphoteric properties and CEC values for the samples were listed in Table 1 and Table S2. For the DBC and its modified samples, a large number of acidic groups were detected (8.35–10.9 mmol/g), but the basic groups were not detected. Specifically, the oxidation treatments elevated the acidic groups from 8.69 to 10.9 mmol/g, but the acid hydrolysis and activation treatments showed a slight decrease in the acidic groups, reaching 8.35 mmol/g. On the

contrary, BC and BC-PM contained more abundant basic groups (8.42 mmol/g and 6.96 mmol/g, respectively), and a few acidic groups such as phenolic hydroxyl groups (1.85 mmol/g and 1.43 mmol/g, respectively). Moreover, the CEC values of black carbon in this investigation were ranging from 99.5 to 188 cmol/kg (Table 1), and the oxidation treatments significantly enhanced the CEC values.

3.3. Nanoporosity and its size distribution

Fig. S3 showed the CO_2 adsorption isotherms and the nanopore size distribution for the samples. The DR model can well fit the adsorption isotherm of CO_2 ($R^2 > 1.00$). Table 2 listed the specific surface areas (SSA) and nanopore volumes (V_o) of the samples. As showed in Table 2, the V_o and SSA of MB were 26.8 μL/g and 66.7 m²/g, respectively. The detailed information of DMB can be found from our group's previous research, which were 35.3 μL/g and 88.1 m²/g, respectively (Hu et al., 2017). For modified black carbon, the SSA and V_o values of samples ranged from 158 to 241 m²/g and from 63.3 to 96.5 μL/g, respectively. Particularly, the values of SSA (241 m²/g) and V_o (96.5 μL/g) of DBC-Z were the highest. But the SSA and V_o values of the other modified DBC samples were reduced to some extent. It was found that a large decrease of SSA and V_o from DBC to DBC-SC, with the SSA and V_o decreasing from 230 m²/g to 158 m²/g and from 92.2 μL/g to 63.3 μL/g, respectively. For the H_2O_2-treated sample, the SSA and V_o decreased obviously to 214 m²/g and to 85.9 μL/g, respectively. But the HCl-treated sample had a slight decrease in the SSA and V_o. In comparison with BC, the removal of a large amount of silicate during the demineralization process resulted in a significant increase in SSA and V_o for DBC, ranging from 177 m²/g to 230 m²/g and from 71.0 μL/g and 92.2 μL/g, respectively (Table 2). After the surface recombination of BC with
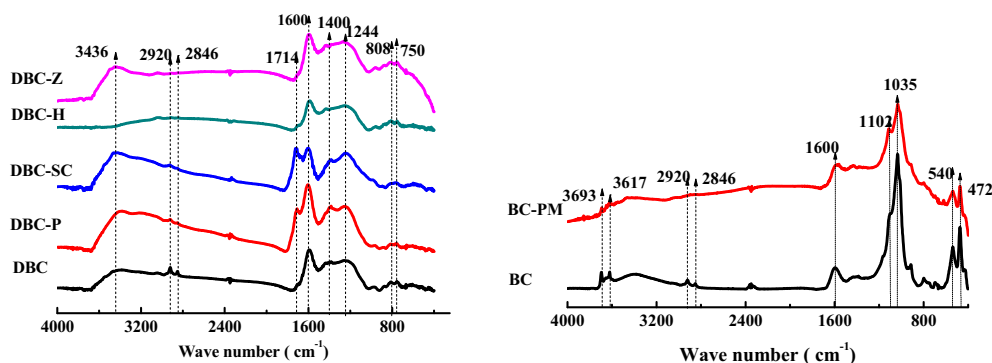
Fig. 1. FTIR spectra of the black carbon and its modified samples.

Table 2
The nanopore volumes and specific surface areas of CO_2 adsorption, and the adsorption volumes (Q_o') of phenanthrene on the black carbon and its modified samples by using different models.

Sample	Dubinin-Radushkevitch		CSA^a m^2/g	SSA^b m^2/g	Cumulative pore volume			Adsorption volumes (Q_o') μL/g			
	V_o μL/g	SSA m^2/g			0–0.7 nm μL/g	0.7–1.1 nm μL/g	1.1–2 nm μL/g	Q_o'-FM, $C_e = S_w$ $(\%)^c$	Q_o'-PD, $(\%)^c$	Q_o'-LPPD, $(\%)^c$	Q_o'-DR, $(\%)^c$
MB	26.8	66.7	36.0	146	7.94	2.60	16.3	–	–	–	–
DMB^d	35.3	88.1	41.6	189	9.50	2.90	22.9	–	–	–	–
$R500^e$	78.9	189	–	–	22.4	8.70	47.8	54.8 (69.5)	–	–	25.0 (31.6)
DBC	92.2	230	182	480	40.9	11.6	39.7	31.8 (34.5)	45.2 (49.1)	26.8 (29.0)	27.5 (27.8)
DBC-P	85.9	214	154	493	35.0	8.10	42.8	65.7 (76.5)	88.2 (103)	70.2 (81.7)	53.8 (62.9)
DBC-SC	63.3	158	119	365	27.0	6.75	29.4	31.2 (49.3)	46.8 (73.9)	26.9 (42.5)	23.4 (36.7)
DBC-H	91.0	227	167	469	39.2	10.1	41.7	49.0 (53.8)	34.8 (38.3)	27.8 (30.5)	41.5 (45.1)
DBC-Z	96.5	241	183	559	42.7	11.3	42.5	26.4 (27.4)	30.8 (31.9)	18.3 (19.0)	23.0 (22.6)
BC	71.0	177	136	371	29.9	10.2	30.9	12.6 (17.7)	12.8 (18.7)	5.99 (8.43)	10.3 (14.3)
BC-PM	70.0	175	142	369	31.3	10.1	28.7	10.3 (14.7)	10.3 (15.2)	4.95 (7.07)	9.02 (12.8)

[a] CSA is cumulative surface area of the sample.
[b] SSA is calculated using nonlocal density functional theory (NLDFT).
[c] (%) is the percentage of Q_o' accounting for the total nanopore volume of CO_2 adsorption.
[d] DMB data comes from Hu et al. (2017).
[e] R500 was the BC samples in our previous investigation, which was exhaustively extracted with three-member solvents (Zhang et al., 2014; Duan et al., 2018).

$KMnO_4$, the SSA and V_o values of BC-PM decreased slightly, ranging from 177 m^2/g to 175 m^2/g and from 71.0 μL/g and 70.0 μL/g, respectively. Moreover, the V_o values were positively correlated with OC% for the samples (Fig. 2).

Fig. S3 showed that the nanopores were mainly concentrated at 0–0.7 nm and 1.1–2 nm. The modified DBC samples including DBC-P, DBC-SC, DBC-H, and DBC-Z showed reduced nanopore size percentages at 0–0.7 nm. After the $KMnO_4$ surface recombination, the nanopore size percentage at 0–0.7 nm increased slightly. In addition, samples without pyrolysis (MB and DMB) have larger nanopore sizes than pyrolysis samples.

3.4. Sorption isotherms of phenanthrene on the samples

Table 3 listed the Freundlich (FM) parameters for the sorption of phenanthrene on black carbon and its modified samples. Fig. S4 showed the sorption isotherms. As showed in Table 3, the FM described all the sorption data well with R^2 ranging from 0.94 to 0.99, and the sorption
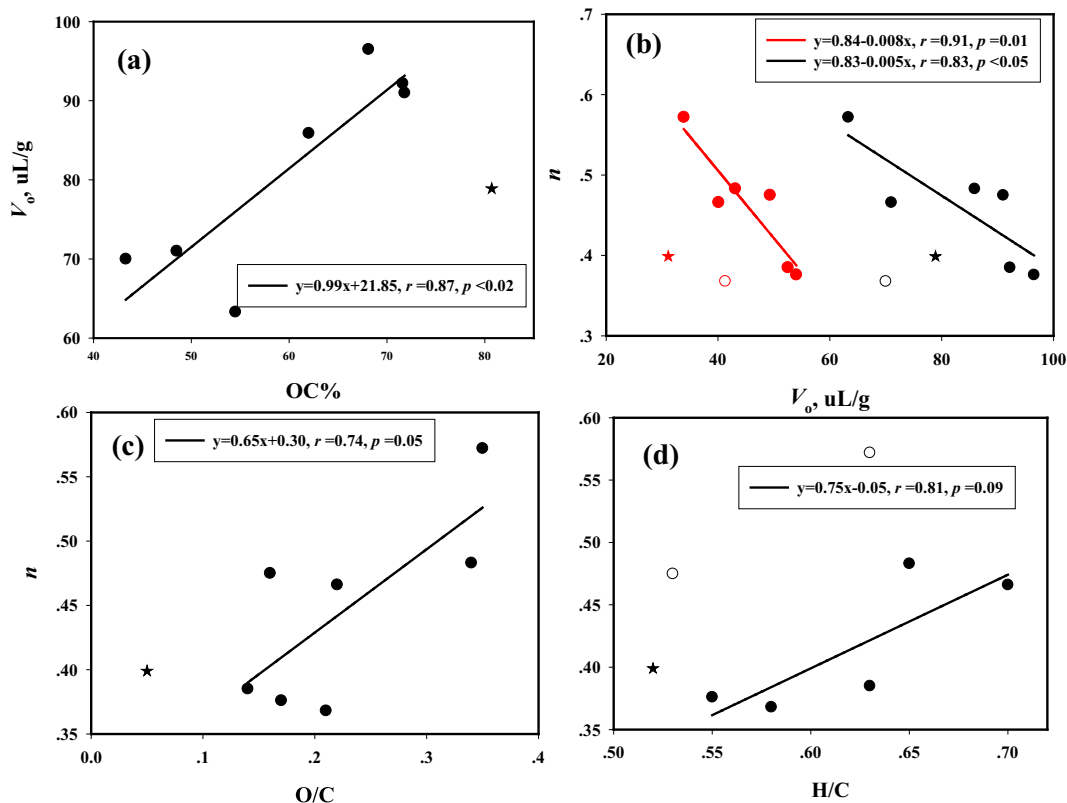
Fig. 2. The correlation of V_o with OC% (a), and the correlations of n with V_o (b), O/C (c), and H/C (d). In panels, the red or black star represents the corresponding data for one similar black carbon sample produced and extracted by mixed solvents (Duan et al., 2018). In b panel, the red dot and black dot represent the V_o at 0–1.1 nm and 0–2 nm, respectively, and the outlier (BC-PM) was showed in blank marks and not included in the correlation equation. In d panel, the outliers (DBC-SC and DBC-H) were showed in the circled dots and not included in the correlation equation.

Table 3
Freundlich model parameters for the Phen sorption on the samples.

Sample	K_F[a]	n	N[b]	R^2	K_{OC}, mL/g	log K_{OC}, mL/g
					$C_e = 0.01S_w$[c]	$C_e = 0.01S_w$[c]
R500[d]	3890	0.399	18	0.94	1,128,617	6.05
DBC	2483	0.385	16	0.99	785,090	5.89
DBC-P	2592	0.483	17	0.99	1,198,458	6.08
DBC-SC	657	0.572	17	0.99	429,006	5.63
DBC-H	2048	0.475	16	0.94	802,104	5.90
DBC-Z	2206	0.376	18	0.99	717,829	5.86
BC	561	0.466	17	0.99	327,570	5.52
BC-PM	909	0.368	17	0.99	456,181	5.66

[a] K_F is the sorption affinity coefficient with units of $(\mu g/g)/(\mu g/L)^n$.
[b] Number of data.
[c] $C_e = 0.01S_w$ means that the concentration of the adsorbate in the solution is one-hundredth of its solubility at room temperature.
[d] R500 was the BC samples in our previous investigation, which was exhaustively extracted with three-member solvents (Zhang et al., 2014; Duan et al., 2018).

was highly nonlinear with n values ranging from 0.368 to 0.572. The oxidation treatment by H_2O_2 and NaClO, as well as the HCl hydrolysis reduced the sorption nonlinearity, with the values of n increasing from 0.385 to 0.572. However, the $ZnCl_2$ activation and $KMnO_4$ treatment strengthened the sorption nonlinearity with n values decreasing from 0.385 to 0.376 and 0.466 to 0.368, respectively. The n values were negatively correlated with V_o at 0–2 nm ($R^2 = 0.83$, $p < 0.05$) and V_o at 0–1.1 nm ($R^2 = 0.91$, $p = 0.01$), and were positively correlated with O/C ($R^2 = 0.74$, $p = 0.05$) and H/C ($R^2 = 0.81$, $p = 0.09$) (Fig. 2). Since FM is not restricted to the monolayer adsorption, and is more

suitable to describing the sorption isotherms, FM was applied to the further result and discussion.

The log K_{OC} (mL/g) values at $C_e = 0.01S_w$ (The concentration of the adsorbate in the solution is one-hundredth of its solubility at room temperature.) ranged from 5.52 to 6.08 in this study (Table 3), and were positively correlated with V_o (1.1–2 nm and 0–2 nm) and SSA (Fig. 3), and were better with V_o at 1.1–2 nm. In addition, except for DBC-P and DBC-SC, there were significant negative correlations between log K_{OC} and (N + O)/C or O/C ratios for the DBC and BC modified samples (Fig. 3). It was found that log K_{OC} values were highly significantly, and negatively related to the surface polarity parameters ((N + O)/C and O/C) determined by XPS or by elemental analysis, especially when the deduction of inorganic oxygen (SiO_2) was conducted. Furthermore, the polarity, aromatic carbon, and/or nanopore properties of the samples were used to establish two multiple factor equations for the sorption affinity. The outliers (DBC-P and DBC-SC) was not included in the correlation equation. The one equation was: log$K_{OC} = 0.412x_1 - 0.793x_2$ ($R^2 = 0.95$, $p = 0.01$). Here, x_1 is the nanopore volume (V_o), x_2 is the polarity index (N + O)/C by elemental analysis, respectively. Another equation was: log$K_{OC} = 0.519x_1 - 0.538x_2$ ($R^2 = 1.00$, $p < 0.01$). Here, x_1 is C—C values calculated by XPS, x_2 is the polarity index (N + O)/C by elemental analysis, respectively. The above results demonstrated the importance of polarity, nanopore, and/or aromatic carbon.

3.5. Nanopore-filling modeling

To investigate the effect of nanopore properties on the sorption of phenanthrene, the FM, PD, $LPPD$, and DR adsorption models were used to calculate the adsorption volumes (Q_o') of phenanthrene. It was
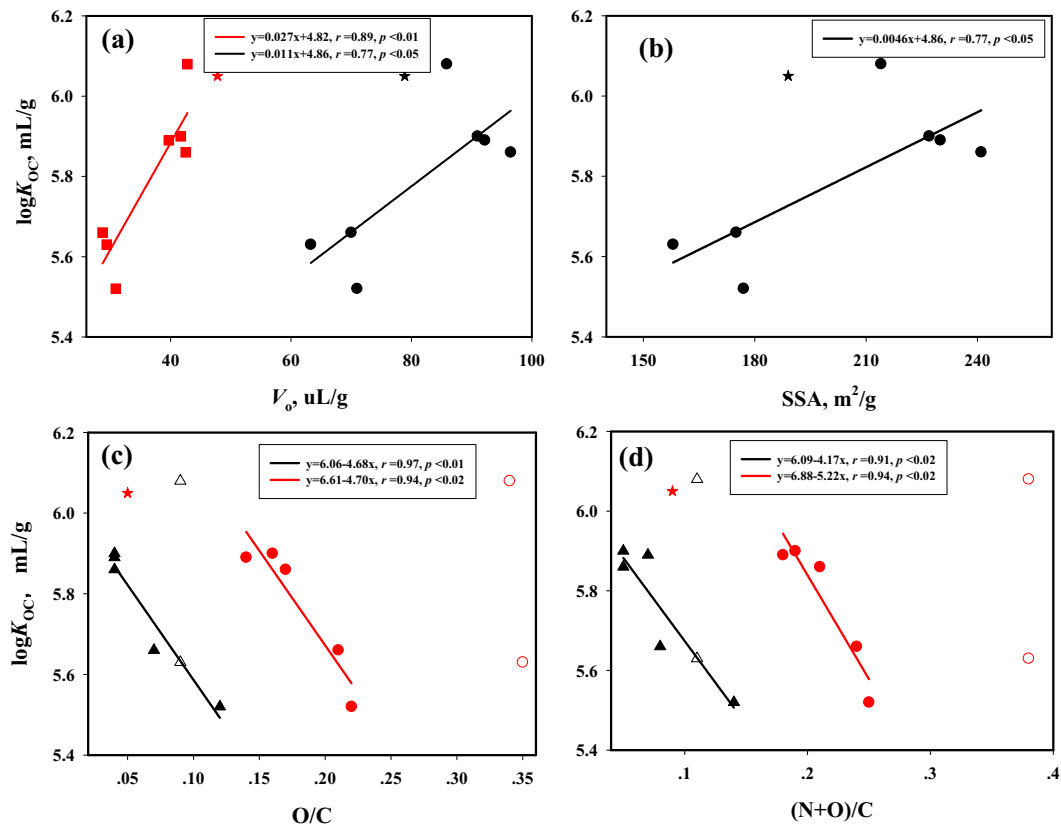
Fig. 3. The correlations of log K_{OC} (mL/g) with nanopore volume (V_o) (a), SSA (b), O/C (c), and (N + O)/C (d). In a panel, the red square and black dot represent the V_o at 1.1–2 nm and 0–2 nm, respectively. The a, b, c, and d panels represents the corresponding data for one similar black carbon sample produced and extracted by mixed solvents (Duan et al., 2018). In c and d panels, triangles represent (N + O)/C and O/C values deducted from the inorganic oxygen (SiO_2) by XPS, and dots represent (N + O)/C and O/C values measured by elemental analysis. The outliers (DBC-P or DBC-SC) were showed in the blank marks and not included in the corresponding correlation equations.

found that these models could well fit the adsorption data (Table S2-S4). Particularly, the correlation coefficients of the *PD* model were the highest with $R^2 \geq 0.99$ (Table S2). Table 2 listed their adsorption volumes of phenanthrene on the samples. The adsorption volumes (Q_o') for FM (values at $C_e = S_w$) ranged from 10.3 to 65.7 μL/g. The b' values and the maximum adsorption volumes (Q_o') fitted by the *PD* model ranged from 1.17 to 2.42 and from 10.3 to 88.2 μL/g, respectively (Table S2). Table S3 illustrated that the Q_o' values for the adsorption curves using the reported K_d values ranged from 4.95 to 70.2 μL/g, and b' values ranged from 1.44 to 3.30. The Q_o' values for the *DR* model ranged from 9.02 to 53.8 μL/g, and the D values ranged from 0.100 to 0.148. It was noted that the Q_o' values for BC and BC-PM were lower than for other samples.

The Q_o' values estimated by the above models were lower than the total nanopore volumes (70.0–96.5 μL/g) measured by the CO_2 adsorption, and the Q_o' values of *PD* were approaching to the total nanopore volumes (Table 2). Specifically, for the DBC and its modification samples, the percentages of Q_o' accounting for V_o ranged from 31.9% to 103% for the *PD* model (Table 2). Moreover, when the DBC-P and DBC-SC were excluded, the correlation of adsorption volumes (Q_o') calculated from different models (*FM*(a), *PD*(b), *LPPD*(c), and *DR*(d)) with V_o (0–2 nm) in Fig. 4 is respectively significant or marginally significant. The slopes of the regression equations range from 0.76 to 1.05, but the intercepts range from 47.1 to 61.7 μL/g, suggesting that more than a half of the nanopore volumes could not be accessed by Phen molecules. In addition, we carried out a multiple linear regression for estimating the effects of different nanopore size. The equations were as follows: $Q_o'_{(FM)} = 1.510x_1 - 1.015x_2$ ($R^2 = 0.92$, $p < 0.01$), $Q_o'_{(PD)} = 1.424x_1 - 1.106x_2$ ($R^2 = 0.79$, $p < 0.05$), $Q_o'_{(LPPD)} = 1.487x_1 - 1.134x_2$ ($R^2 =$ 0.86, $p < 0.02$), and $Q_o'_{(DR)} = 1.480x_1 - 0.925x_2$ ($R^2 = 0.91$, $p < 0.01$). Here, x_1 is the nanopore volume at 1.1–2 nm, x_2 is the nanopore volume at 0–1.1 nm.

4. Discussion

4.1. Surface and structural properties of the samples

In this study, either element analysis, infrared analysis, surface element analysis (XPS), or surface amphoteric analysis, have shown that the oxidation treatment introduced some oxygen-containing functional groups, and acid hydrolysis or activation treatment demonstrated the partial decomposition of DBC. It was reported that the —COOH and C—O groups were majorly associated with aromatic carbon groups (Ran et al., 2007). Hence, the sorption parameters and nanopore-filling volumes of Phen on DCB-SC and DCB-P were highly changed, as showed in Figs. 2, 3, and 4. In previous investigation, Paul et al. (2006) and Simpson et al. (2003) suggested that acid hydrolysis can remove a portion of esters, amines and saccharides from humus and soil organic carbon. Zhang et al. (2011) and Liu et al. (2015) illustrated the introduction of oxygen-containing functional groups during oxidation process. The lower H/C or O/C ratios of the BC sample were related to the fact that some of the aliphatic or polar carbon structure disappeared during the thermal evolution, resulting in a lower aliphaticity and polarity (Duan et al., 2018; Zhang et al., 2014). In addition, surface elemental analysis (XPS) and IR spectrum analysis showed that a large amount of silicate removal occurred during the demineralization treatment (Qian et al., 2015; Xiao et al., 2014; Rumpel et al., 2006) for DBC. Besides, the presence of C—O absorption peaks of esters or lactones (Song et al.,
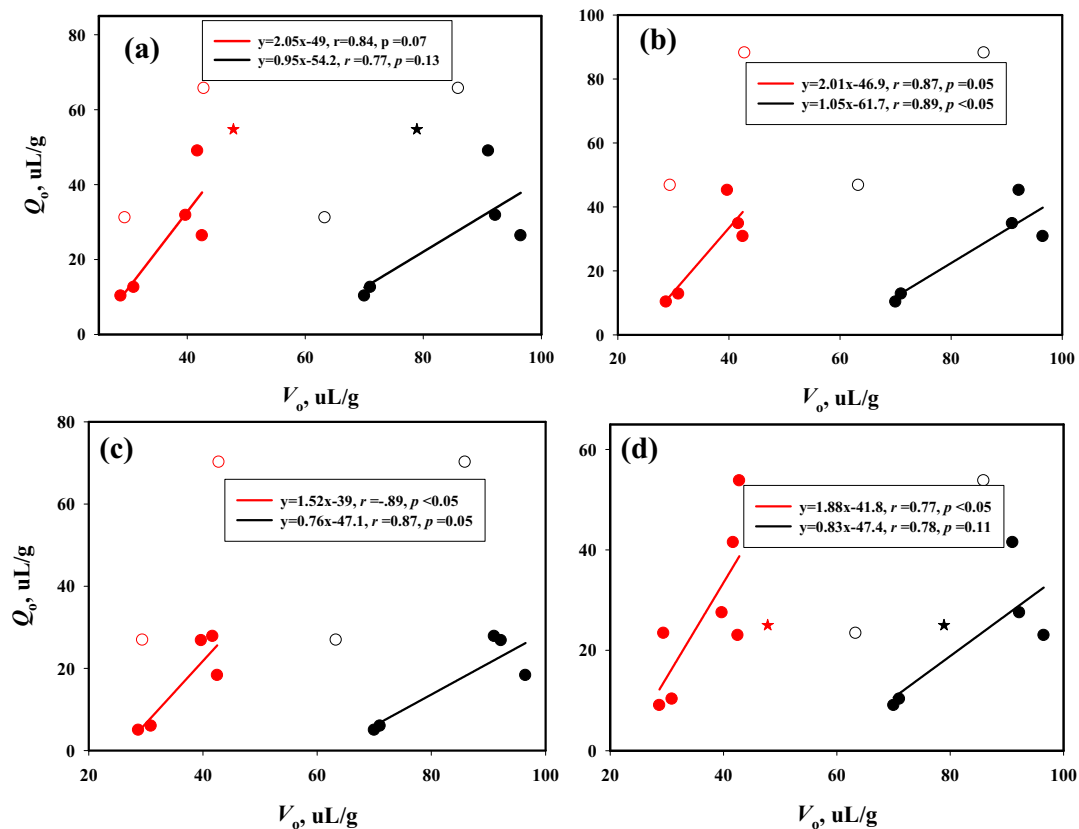
Fig. 4. The correlations of adsorption volumes (Q_o') calculated from different models (*FM*(a), *PD*(b), *LPPD*(c), and *DR*(d)) with V_o. The red and black dots represent the V_o at 1.1–2 nm and 0–2 nm, respectively, and the outliers (DBC-P or DBC-SC) was showed in blank marks and not included in the correlation equation. The star represents the adsorption volume derived from the *FM* and *DR* model for the similar black carbon sample extracted by solvents in previous investigation (Duan et al., 2018).

2014) and the removal of a large amount of silicate in BC-PM revealed that the decrease of total O content (Table 1) was partially related to the decrease of Si—O during the KMnO$_4$ treatment.

The surface amphoteric properties and CEC values for the samples in Table 1 and Table S2 indicated that our samples had higher surface amphoteric groups (1.43–10.9 mmol/g, Table 1) than those of biomass derived BCs (0.24–8.1 mmol/g) (Wang et al., 2013; Mukherjee et al., 2011). Moreover, the black carbon in this investigation gave higher CEC values ranging from 99.5 to 188 cmol/kg (Table 1) than biomass derived black carbon produced at 500 °C or 600 °C (1.3–34.8 cmol/kg) did (Wang et al., 2013; Lehmann et al., 2011; Mukherjee et al., 2011). Previous report has found that the oxidation treatments significantly enhanced the CEC values (Cheng et al., 2006). Likewise, our H$_2$O$_2$-treated sample gave a much higher CEC value of 188 cmol/kg than the reported values (1.3–34.8 cmol/kg). Lehmann et al. (2011) and Liang et al. (2006) showed that the addition of oxidized black carbon to the soil could increase the CEC values of the soil and had better agricultural applications. Hence, the above results clearly revealed the improvement of surface properties and cation exchange capacity on the modified black carbon samples.

In addition to the surface properties, the nanopore properties of samples in Table 2 illustrated the change of nanopore volumes and nanopore size distribution on the modified black carbon samples. It was found that oxidation treatment reduced the SSA and V_o values of the samples strongly, especially for NaClO treatment. This observation was consistent with the previous investigation suggesting that the SSA values of bleached samples (16.6–402.1 m^2/g) were smaller than those of unbleached samples (155.0–544.6 m^2/g) (Han et al., 2014). On the one hand, the reduction of organic matter will lead to the reduction of nanopores; on the other hand, partial removal of organics (aromatic groups) will result in the destruction of the nanopores structure, which will change nanopore size distribution, resulting in a reduction in the nanopore volume and surface area of the BC, as other investigators also observed (Liu et al., 2012; Mikutta et al., 2005). But the HCl-treated sample had a slight decrease in SSA and V_o, similar to the previous study. In the previous investigation on 700 BCE and 400 BCE, the surface areas were reduced from 292 m^2/g to 152 m^2/g by the HCl hydrolysis (Zhang et al., 2011). Besides, although the SSA value of DBC-Z increased to 241 m^2/g, it was lower than 500 m^2/g reported in a previous study on activated carbon with a carbonization time of 60 min and a chemical ratio of 100% with ZnCl$_2$ at 500 °C (Mohanty et al., 2005). Simultaneously, another investigation also found that surface area of activated carbon produced by ZnCl$_2$ for rice straw at 850 °C reached up to 1442 m^2/g (He et al., 2013). The above difference may be attributed to various treatments. Moreover, the correlation between V_o and OC% (Fig. 2) indicated that organic matter was the dominating matrix to produce nanopores. In comparison with one previous investigation, the V_o-OC correlation for the similar BC sample extracted by mixed organic solvents was similar, suggesting that the effect of by-product (tar, polycyclic aromatic hydrocarbons (PAHs), etc) was insignificant (the red or black star in Fig. 2). The above results clearly illustrated the change of surface and structural properties of the modified samples.

4.2. Sorption parameters and sorption mechanism

The relationship of sorption nonlinearity (n) with nanopore volume (V_o), H/C, and O/C (Fig. 2) suggested that the change of aromaticity and nanopore size after different modification, especially at the nanopore size of 0–1.1 nm, contributed to the sorption nonlinearity. Previous investigation has shown that the existence of intragrain microporosity may be responsible for the nonlinearity sorption (Sun et al., 2013). On the other hand, one previous investigation showed that as the maturity increased, the O/C and H/C values became smaller, and the aromaticity became stronger, resulting in a stronger nonlinear sorption (Duan et al., 2018; Zhang et al., 2014). In addition, the relationship of sorption

affinity (log K_{OC}) with nanopore volume (V_o) and SSA (Fig. 3), as well as the above multiple factor equations, indicated that nanopore volume was the crucial factor in the sorption of phenanthrene. Furthermore, in comparison with one previous investigation, the similar BC samples extracted with three organic solvents (the red and black stars in Figs. 2 and 3) gave the similar correlation, indicating that the by-products such as tar and PAHs had a negligible effect on the sorption behavior of phenanthrene (Duan et al., 2018).

The log K_{OC} (mL/g) values (5.52–6.08) in this investigation (Table 3) were higher than those (5.11–5.85) of biomass-derived biochar produced at 500 °C or even at 600 °C (Han et al., 2014; Wang et al., 2016). At the same time, the surface area and nanopore volume of these biomass-derived biochar were 257.2–620.3 m^2/g and 57–119 μL/g, respectively. Hence, the kerogen-derived black carbon and its modified samples in this investigation had higher sorption affinity to phenanthrene. On the one hand, SSA in Han's and Wang's study was calculated using nonlocal density functional theory (NLDFT), which is different from our study (DR). When we used NLDFT model, the SSA values was 365–559 m^2/g (Table 2), which were similar to or slightly lower than Han's and Wang's data. Our higher logK_{OC} values may be related to the old biological materials. On the other hand, the aromatic interlayer spacing decreased when temperature reached 450 °C, as demonstrated in previous investigations of our group (Zhang et al., 2014; Duan et al., 2018). That may account for their lower logK_{OC} values of Phen on the BC samples produced at 600 °C than on our BC samples although they obtained higher V_o and SSA values.

The increase of polarity in this investigation did not reduce the sorption affinity of DBC-P. The increase of graphite interlayer spacing during the oxidation process may also be responsible for the increase of adsorption capacity for DBC-P. Other investigators reported that the surface oxygen-containing functional groups can improve the hydrophilicity of BC, which facilitates its dispersion in the aqueous phase and the adsorption of contaminants in the aqueous phase (Liu et al., 2015). After the NaClO oxidation, the K_{OC} values of phenanthrene decreased by 45.4% (Table 3), presumably due to significant reduction of nanopore volume and specific surface area, as well as the increasing polarity. The observation was consistent with pervious study, which reported that the sorption affinity of phenanthrene and pyrene was reduced greatly by the NaClO treatment, and K_{OC} decreased by 61.4% and 43.1%, respectively (Huang et al., 2006). For the activation treatment with ZnCl$_2$, K_{OC} values decreased by 8.57% (Table 3). Although the nanopore volume for DBC-Z increased, the increase of polarity may reduce its sorption affinity of phenanthrene. Furthermore, when BC was treated with KMnO$_4$, its sorption affinity was enhanced, but its nanopore volume and specific surface area did not change significantly. The above results and analyses suggested that the importance of nanoporosity, surface areas, and polar functional groups in the sorption of phenanthrene by the samples. It was noted that the importance of surface area, pore size distribution, and surface functionality to the sorption of HOCs by black carbon were also reported in a previous report (Zhu et al., 2005).

The adsorption volume (Q_o') in Table 2 further revealed the contribution of the nanopore volume to sorption of phenanthrene. In addition, the relationship between Q_o' and V_o, as well as the above multiple linear regressions for different nanopore size, indicated that nanopore filling was the main sorption mechanism and the molecular sieve effect occurred in the sorption. The small-sized CO$_2$ molecules (0.253 nm) are more accessible to relatively small nanopores than the large-sized phenanthrene molecules (0.341 nm × 0.999 nm × 1.094 nm) (Duan et al., 2018). The molecular sieve effect can underestimate the nanopore filling volumes of the modified black carbon (Table 2). Moreover, previous studies have shown that for kerogen samples at low and medium degree of catagenesis, the interlayer spacings are widely spread (0.34–>0.8 nm). However, the nonaromatic groups begin to disappear and the interlayer space spreading decreases for the similar BC samples used in this investigation (Ran et al., 2004; Oberlin et al., 1980). The

above analyses suggested that adsorption (nanopore filling) is the dominant sorption mechanism of phenanthrene by the investigated samples, demonstrating the importance of the adsorption mechanism in the sorption of HOCs. As demonstrated above, the existence of internal nanoporosity in the samples is also responsible for the nonlinearity of the phenanthrene sorption isotherms.

5. Conclusions

The surface properties, structural properties, and sorption isotherms of phenanthrene on the black carbon and its modified samples were investigated in this study. Oxidation treatments (H_2O_2 and NaClO) enhanced the cation exchange capacities, acidic oxygen functional groups, surface polarity, etc., but reduced the nanopore volumes. However, the sorption affinity of phenanthrene by these samples was variable, illustrating that the sorption was affected by various factor. Acid hydrolysis (HCl) had insignificant effect on the surface properties, structural properties, and sorption behavior of phenanthrene. Nevertheless, the activation treatment ($ZnCl_2$) elevated the nanopore volume of the sample. Surface recombination ($KMnO_4$) enhanced the cation exchange capacities, acidic oxygen functional groups, surface polarity, nanopore volumes, and sorption affinity of phenanthrene. It was found that the sorption affinity parameters log K_{OC} of phenanthrene were positively correlated with SSA and V_o ($p < 0.05$), and the n values were negatively correlated with V_o ($p < 0.05$), respectively, indicating that the nanopore and surface structure of BC and DBC led to the difference in the sorption behaviors of phenanthrene. The nanopore modeling showed that the nanopore filling was the main sorption mechanism of phenanthrene on the black carbon and its modified samples, and the molecular sieve effects were observed in the sorption of phenanthrene. Moreover, the BC yields are much higher in this investigation than in other investigations. However, as the raw biological materials (old vs. fresh) used are quite different, more investigations need to be conducted to compare the sorption behaviors, sorption mechanism, and production ratios, carbon sequestration of different BCs in soils and sediments, etc.

Appendix A. Supplementary data

One table shows the weights and OC recoveries of the modified BC and DBC, one table shows the elemental composition and chemical properties of the samples, and three tables show the *PD*, *LPPD*, and *DR* model fitting parameters, respectively. Three figures show the X-ray photoelectron spectra (XPS) and C1s spectra scanning, and CO_2 sorption isotherms and nanopore size distribution, and one figure shows the sorption isotherms by different models.

References

Accardi-Dey, A., Gschwend, P.M., 2002. Assessing the combined roles of natural organic matter and black carbon as sorbents in sediments. Environ. Sci. Technol. 36, 21–29.

Ahmadpour, A., Do, D., 1997. The preparation of activated carbon from macadamia nutshell by chemical activation. Carbon 35, 1723–1732.

Ahmedna, M., Marshall, W.E., Husseiny, A.A., Rao, R.M., Goktepe, I., 2004. The use of nutshell carbons in drinking water filters for removal of trace metals. Water Res. 38, 1062–1068.

Boehm, H.P., 1994. Some aspects of the surface chemistry of carbon blacks and other carbons. Carbon 32 (5), 759–769.

Chefetz, B., Xing, B., 2009. Relative role of aliphatic and aromatic moieties as sorption domains for organic compounds: a review. Environ. Sci. Technol. 43, 1680–1688.

Cheng, C.H., Lehmann, J., Thies, J.E., Burton, S.D., Engelhard, M.H., 2006. Oxidation of black carbon by biotic and abiotic processes. Org. Geochem. 37, 1477–1488.

Cheng, C.H., Lin, T.P., Lehmann, J., Fang, L.J., Yang, Y.W., Menyailo, O.V., Chang, K.H., Lai, J.S., 2014. Sorption properties for black carbon (wood char) after long term exposure in soils. Org. Geochem. 70, 53–61.

Chun, Y., Sheng, G., Chiou, C.T., Xing, B., 2004. Compositions and sorptive properties of crop residue-derived chars. Environ. Sci. Technol. 38, 4649–4655.

Di Blasi, C., Branca, C., Galgano, A., Zenone, F., 2015. Modifications in the thermicity of the pyrolysis reactions of $ZnCl_2$-loaded wood. Ind. Eng. Chem. Res. 54, 12741–12749.

Duan, D., Zhang, D., Ma, X., Yang, Y., Ran, Y., Mao, J., 2018. Chemical and structural characterization of thermally simulated kerogen and its relationship with microporosity. Mar. Pet. Geol. https://doi.org/10.1016/j.marpetgeo.2016.12.016.

Girgis, B.S., Yunis, S.S., Soliman, A.M., 2002. Characteristics of activated carbon from peanut hulls in relation to conditions of preparation. Mater. Lett. 57, 164–172.

Guo, X., Miao, Y., Yang, C., Zhang, Q., Gao, L., Hu, Y., 2016. Sorption of tylosin on black carbon from different sources. J. Environ. Chem. Eng. 4, 3393–3400.

Gustafsson, Ö., Haghseta, F., Chan, C., MacFarlane, J., Gschwend, P.M., 1996. Quantification of the dilute sedimentary soot phase: implications for PAH speciation and bioavailability. Environ. Sci. Technol. 31, 203–209.

Han, L., Sun, K., Jin, J., Wei, X., Xia, X., Wu, F., Gao, B., Xing, B., 2014. Role of structure and microporosity in phenanthrene sorption by natural and engineered organic matter. Environ. Sci. Technol. 48, 11227–11234.

He, X., Ling, P., Yu, M., Wang, X., Zhang, X., Zheng, M., 2013. Rice husk-derived porous carbons with high capacitance by $ZnCl_2$ activation for supercapacitors. Electrochim. Acta 105, 635–641.

Hu, S.J., Zhang, D.N., Xiong, Y.Q., Yang, Y., Ran, Y., 2017. Adsorption of phenanthrene and nonylphenol by different activated and oxidized kerogen at room temperature. Acta Sci. Circumst. 37 (10), 3720–3828 (In Chinese).

Huang, L., Boving, T.B., Xing, B., 2006. Sorption of PAHs by aspen wood fibers as affected by chemical alterations. Environ. Sci. Technol. 40, 3279–3284.

ISO 11260–1997, 1997. Determination of effective cation exchange capacity and base saturation level using barium chloride solution.

Jonker, M.T., Koelmans, A.A., 2002. Sorption of polycyclic aromatic hydrocarbons and polychlorinated biphenyls to soot and soot-like materials in the aqueous environment: mechanistic considerations. Environ. Sci. Technol. 36, 3725–3734.

Kleineidam, S., Schüth, C., Grathwohl, P., 2002. Solubility-normalized combined adsorption-partitioning sorption isotherms for organic pollutants. Environ. Sci. Technol. 36, 4689–4697.

Lehmann, J., Rillig, M.C., Thies, J., Masiello, C.A., Hockaday, W.C., Crowley, D., 2011. Biochar effects on soil biota–a review. Soil Biol. Biochem. 43, 1812–1836.

Liang, B., Lehmann, J., Solomon, D., Kinyangi, J., Grossman, J., O'Neill, B., Skjemstad, J.O., Thies, J., Luizão, F.J., Petersen, J., 2006. Black carbon increases cation exchange capacity in soil. Soil Sci. Soc. Am. J. 70, 1719–1730.

Linares, N., Silvestre-Albero, A.M., Serrano, E., Silvestre-Albero, J., Garcia-Martinez, J., 2014. Mesoporous materials for clean energy technologies. Chem. Soc. Rev. 43, 7681–7717.

Liu, Z.H., Qiu, J.R., Tan, Z.Q., Zeng, H.C., Liu, H., Hu, X., Zhang, M.N., 2012. Experimental study of NO removal by modified activated carbon fiber. Proc. CSEE 32 (8), 64–70 (In Chinese).

Liu, W.J., Jiang, H., Yu, H.Q., 2015. Development of biochar-based functional materials: toward a sustainable platform carbon material. Chem. Rev. 115, 12251–12285.

Lutfalla, S., Chenu, C., Barré, P., 2014. Are chemical oxidation methods relevant to isolate a soil pool of centennial carbon? Biogeochemistry 118, 135–139.

Mikutta, R.M., Kaiser, K., 2011. Organic matter bound to mineral surfaces: resistance to chemical and biological oxidation. Soil Biol. Biochem. 43, 1738–1741.

Mikutta, R.M., Kleber, M., Kaiser, K., Jahn, R., 2005. Review: organic matter removal from soils using hydrogen peroxide, sodium hypochlorite, and disodium peroxodisulfate. Soil Sci. Soc. Am. J. 69 (1), 120–135.

Mohanty, K., Das, D., Biswas, M., 2005. Adsorption of phenol from aqueous solutions using activated carbons prepared from *Tectona grandis* sawdust by $ZnCl_2$ activation. Chem. Eng. J. 115, 121–131.

Mukherjee, A., Zimmerman, A.R., Harris, W., 2011. Surface chemistry variations among a series of laboratory-produced biochars. Geoderma 163, 247–255.

Nguyen, T.H., Cho, H.H., Poster, D.L., Ball, W.P., 2007. Evidence for a pore-filling mechanism in the adsorption of aromatic hydrocarbons to a natural wood char. Environ. Sci. Technol. 41, 1212–1217.

Oberlin, A., Boulmier, J.L., Villey, M., 1980. Electron Microscopic Study of Kerogen Microtexture. Selected Criteria for Determining the Evolution Path and Evolution Stage of Kerogen. Kerogen: Insoluble Organic Matter from Sedimentary Rocks. Editions Technip, Paris, pp. 191–241.

Paul, E.A., Morris, S.J., Conant, R.T., Plante, A.F., 2006. Does the acid hydrolysis–incubation method measure meaningful soil organic carbon pools? Soil Sci. Soc. Am. J. 70, 1023–1035.

Paul, S., Veldkamp, E., Flessa, H., 2008. Differential response of mineral-associated organic matter in tropical soils formed in volcanic ashes and marine tertiary sediment to treatment with HCl, NaOCl, and $Na_4P_2O_7$. Soil Biol. Biochem. 40, 1846–1855.

Qian, L., Chen, M., Chen, B., 2015. Competitive adsorption of cadmium and aluminum onto fresh and oxidized biochars during aging processes. J. Soils Sediments 15, 1130–1138.

Ran, Y., Xing, B., Rao, P.S.C., Fu, J., 2004. Importance of adsorption (hole-filling) mechanism for hydrophobic organic contaminants on an aquifer kerogen isolate. Environ. Sci. Technol. 38, 4340–4348.

Ran, Y., Sun, K., Yang, Y., Xing, B., Zeng, E., 2007. Strong sorption of phenanthrene by condensed organic matter in soils and sediments. Environ. Sci. Technol. 41, 3952–3958.

Ran, Y., Yang, Y., Xing, B., Pignatello, J.J., Kwon, S., Su, W., Zhou, L., 2013. Evidence of micropore filling for sorption of nonpolar organic contaminants by condensed organic matter. J. Environ. Qual. 42, 806–814.

Rumpel, C., Rabia, N., Derenne, S., Quenea, K., Eusterhues, K., Kögel-Knabner, I., Mariotti, A., 2006. Alteration of soil organic matter following treatment with hydrofluoric acid (HF). Org. Geochem. 37, 1437–1451.

Schmidt, M.W., Noack, A.G., 2000. Black carbon in soils and sediments: analysis, distribution, implications, and current challenges. Glob. Biogeochem. Cycles 14, 777–793.

Shi, L., Zhang, G., Wei, D., Yan, T., Xue, X., Shi, S., Wei, Q., 2014. Preparation and utilization of anaerobic granular sludge-based biochar for the adsorption of methylene blue from aqueous solutions. J. Mol. Liq. 198, 334–340.

Simpson, M.J., Chefetz, B., Hatcher, P.G., 2003. Phenanthrene sorption to structurally modified humic acids. J. Environ. Qual. 32, 1750–1758.

Siregar, A., Kleber, M., Mikutta, R., Jahn, R., 2005. Sodium hypochlorite oxidation reduces soil organic matter concentrations without affecting inorganic soil constituents. Eur. J. Soil Sci. 56, 481–490.

Song, Z., Lian, F., Yu, Z., Zhu, L., Xing, B., Qiu, W., 2014. Synthesis and characterization of a novel MnOx-loaded biochar and its adsorption properties for Cu^{2+} in aqueous solution. Chem. Eng. J. 242, 36–42.

Sun, K., Ran, Y., Yang, Y., Xing, B., Mao, J., 2013. Interaction mechanism of benzene and phenanthrene in condensed organic matter: importance of adsorption (nanopore-filling). Geoderma 204, 68–74.

Wang, Y., Hu, Y., Zhao, X., Wang, S., Xing, G., 2013. Comparisons of biochar properties from wood material and crop residues at different temperatures and residence times. Energy Fuel 27, 5890–5899.

Wang, F., Haftka, J.J.H., Sinnige, T.L., Hermens, J.L., Chen, W., 2014. Adsorption of polar, nonpolar, and substituted aromatics to colloidal graphene oxide nanoparticles. Environ. Pollut. 186, 226–233.

Wang, Z., Han, L., Sun, K., Jin, J., Ro, K.S., Libra, J.A., Liu, X., Xing, B., 2016. Sorption of four hydrophobic organic contaminants by biochars derived from maize straw, wood dust and swine manure at different pyrolytic temperatures. Chemosphere 144, 285–291.

Xiao, X., Chen, B., Zhu, L., 2014. Transformation, morphology, and dissolution of silicon and carbon in rice straw-derived biochars under different pyrolytic temperatures. Environ. Sci. Technol. 48, 3411–3419.

Xu, X., Sun, H., Simpson, M.J., 2010. Concentration and time-dependent sorption and desorption behavior of phenanthrene to geosorbents with varying organic matter composition. Chemosphere 79, 772–778.

Zhang, W., Wang, L., Sun, H., 2011. Modifications of black carbons and their influence on pyrene sorption. Chemosphere 85, 1306–1311.

Zhang, D., Ran, C., Yang, Y., Ran, Y., 2013. Biosorption of phenanthrene by pure algae and field-collected planktons and their fractions. Chemosphere 93, 61–68.

Zhang, Y., Ma, X., Ran, Y., 2014. Sorption of phenanthrene and benzene on differently structural kerogen: important role of micropore-filling. Environ. Pollut. 185, 213–218.

Zhang, D., Ran, Y., Cao, X., Mao, J., Cui, J., Schmidt-Rohr, K., 2015. Biosorption of nonylphenol by pure algae, field-collected planktons and their fractions. Environ. Pollut. 198, 61–69.

Zhang, D., Duan, D., Huang, Y., Xiong, Y., Yang, Y., Ran, Y., 2016. Role of structure, accessibility and microporosity on sorption of phenanthrene and nonylphenol by sediments and their fractions. Environ. Pollut. 219, 456–465.

Zhu, D., Pignatello, J.J., 2005. Characterization of aromatic compound sorptive interactions with black carbon (charcoal) assisted by graphite as a model. Environ. Sci. Technol. 39, 2033–2041.

Zhu, D., Kwon, S., Pignatello, J.J., 2005. Adsorption of single-ring organic compounds to wood charcoals prepared under different thermochemical conditions. Environ. Sci. Technol. 39, 3990–3998.